

Flexible Fiber in a Turbulent Flow: A Macroscopic Polymer

C. Brouzet, G. Verhille,* and P. Le Gal

IRPHE—UMR 7342, CNRS, Aix Marseille Université, Centrale Marseille 49 Rue F. Joliot Curie, 13384 Marseille, France

(Received 2 August 2013; published 20 February 2014)

We describe, for the first time, an experiment devoted to the study of the spatial conformation of a flexible fiber in a turbulent flow. We propose a model for the transition from rigid to flexible regimes as the intensity of turbulence is increased or the elastic energy of the fiber is decreased. This transition occurs for a fiber typical length which is observed experimentally and recovered by our analysis. We also demonstrate that the conformations of flexible fibers in a turbulent flow are analog to conformations of flexible polymers in a good solvent. This last result opens some new and creative ways to model flexible fiber distortions in turbulent flows while addressing fundamental problems in polymer dynamics.

DOI: 10.1103/PhysRevLett.112.074501

PACS numbers: 47.27.-i, 46.70.Hg, 47.57.Ng

The understanding of inertial particle dynamics in turbulent flows is a fundamental issue of hydrodynamics with various applications going from the dispersion of pollutants in air [1] to the transport of pulp fibers in the paper-making industry [2]. Until now, most fundamental works focused on spherical particles and only a few investigations have been done on anisotropic particles such as spheroids, fibers, etc. Moreover, these investigations were mainly concerned with rigid bodies and focused on particle orientation dynamics or on its statistical distribution [3–5] for particles smaller or of the order of the Kolmogorov length $\eta_K = (\nu^3/\epsilon)^{1/4}$, where ϵ is the injected power by unit mass and ν the kinematic viscosity of the fluid. However, for an anisotropic particle with high aspect ratio, its flexibility may strongly affect its motion as the bending energy scales as Ed^4/L [6], where d and L are the diameter and the length of the particle. To understand the particle dynamics, we need not only to study the evolution of its orientation and its center of mass but also analyze and model its spatial conformation. In this Letter, we address several questions: What is the minimal length for a fiber to be distorted by a turbulent flow? When can we neglect its flexibility in turbulence? How can we model its distortion? To answer these questions, we claim that a long enough flexible fiber in a turbulent flow behaves in a similar way to a polymer in a good solvent [7].

The turbulent von Kármán flow used here to generate turbulence is created by the counterrotation of two disks of diameter $2R = 17.2$ cm, fitted with six straight blades (5 mm high). These disks are set 17.6 cm apart at the ends of a cylindrical 18 cm diameter container [cf. Fig. 1(a)]. The mean flow is composed of two toroidal cells rotating in opposite directions separated by an intense shear layer in the midplane. Centrifugal forces close to each disk add two poloidal recirculations [8]. To avoid optical distortions at the air-cylinder interface, this cylinder is immersed inside a cubic box, filled with the working fluid (water if not specified). Experimentally, the rotation frequency F varies

between 2 and 30 Hz so that the integral Reynolds number $Re = 2\pi R^2 F/\nu$ ranges from 10^5 to 1.4×10^6 . The Kolmogorov length η_K determined by the measurement of the injected power ϵ ranges between 12 and 91 μm . Different fibers, whose characteristics are given in Table I, are then introduced individually inside the turbulent flow. The filament is advected by the flow at large scale and is distorted by the turbulent flow. All of the analysis will be performed on fibers located in the central part of the flow where turbulence is nearly homogeneous and isotropic [9]; see Fig. 1(b). Increasing the length of the fiber from 1 to 18 cm allows the observation of two regimes: the rigid

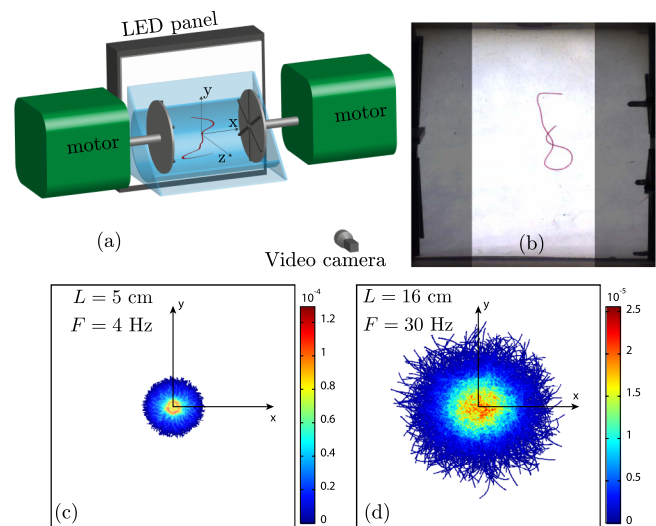


FIG. 1 (color online). (a) Experimental setup. (b) Definition of the working area: only images where the center of mass of the fiber is outside of the shaded regions are considered. (c), (d) Superimposition of all conformations of a type II fiber, 5 cm long, at $F = 4$ Hz (rigid regime) and 16 cm long, at $F = 16$ Hz (flexible regime). The color is proportional to the probability of finding an element of the fiber at the considered position.

TABLE I. Mechanical properties of fibers, with E the Young modulus, ρ_f the density, d the diameter, and L the length.

Type	Material	E (MPa)	ρ_f ($\text{kg} \cdot \text{m}^{-3}$)	d (μm)	L min-max (cm)
I	Silicone	21	1350	900	1.1–17.6
II	Silicone	15	1350	620	1.1–16
III	Nylon	1240	1240	410	1.1–17.6

regime for the shortest fibers and the flexible regime for the longest ones. To understand the transition between both regimes, a systematic study is performed by changing the mechanical properties of the fiber, cf. Table I.

The end-to-end vector $\vec{R}_{e,3D}$, defined as the vector linking the two ends of the filament, is used to characterize the evolution of fiber conformation as its length L or the rotation frequency F is increased. This vector is widely used in polymer science where several models have been drawn to characterize its evolution when the number N of monomers increases [10,11]. In our experiment, only the projection of this vector on the $(x-y)$ plane is measured, cf. Fig. 1(a), with an IDS UI-5240CP 1.3 Mpixel camera. The exposure time is set to 0.2 ms and the acquisition rate is equal to the rotation frequency F , as we are only interested here in the conformation statistics. The fiber is thus easily detected by a classical contrast threshold technique. As the turbulent forcing is invariant by any rotation around the x axis [cf. Fig. 1(a)], it is natural to assume that the statistics of the end-to-end vector shares the same symmetry. Consequently, measuring the end-to-end vector in the $(x-y)$ plane is enough to determine the statistics of the fiber conformations. To validate our assumption, we superimpose all the recorded projected conformations of a filament of a given length and for a fixed frequency where its barycenter is moved to the origin of the $(x-y)$ plane.

Two typical examples are shown in Figs. 1(c) and 1(d) which exhibit a quite good isotropy. This result proves first the homogeneity and isotropy of the turbulence in the working area which is reflected on the symmetry of the system, then that statistically the projection of the center of mass is also the barycenter \vec{r}_b of the filament projection.

First, we focus on the evolution of the mean square value of the end-to-end vector $\langle R_e^2 \rangle$ when the fiber length L is increased whereas the rotation frequency F is fixed; here, $\langle \cdot \rangle$ corresponds to a time average. It is easy to show that the mean value in the 2D plane is proportional to the real norm $\langle R_{e,3D}^2 \rangle$. Indeed, the mean value of the norm $\langle v_{2D}^2 \rangle$ of the projection in the $(x-y)$ plane of a random isotropic vector $\vec{v} = (v \sin \theta \cos \varphi, v \sin \theta \sin \varphi, v \cos \theta)$ is

$$\langle v_{2D}^2 \rangle = \frac{1}{4\pi} \int_{\theta=0}^{\theta=\pi} \int_{\phi=0}^{\phi=2\pi} (v_x^2 + v_y^2) \sin \theta d\theta d\phi \quad (1)$$

$$= \frac{1}{4\pi} \int_{\theta=0}^{\theta=\pi} \int_{\phi=0}^{\phi=2\pi} v^2 \sin^3 \theta d\theta d\phi = \frac{2}{3} v^2. \quad (2)$$

We used here spherical coordinates for simplicity: θ is defined by the angle between \vec{v} and the z axis and φ by the angle between the projection of \vec{v} in the $(x-y)$ plane and the x axis. In Fig. 2(a), one can see that the smallest fibers ($L \lesssim 3$ cm) behave in a rigid manner, implying that $\langle R_e^2 \rangle = 2L^2/3$, as shown by the dashed line. If the length of the fiber is increased, this linear behavior no longer holds, as $\langle R_e^2 \rangle^{1/2}$ is always smaller than the fiber length L . This reflects the distortion of the fiber by turbulent fluctuations. Similar results can be drawn if we consider the radius of gyration R_g defined by $R_g^2 = (1/L) \int (\vec{r} - \vec{r}_b)^2 ds$, where \vec{r} is the current position along the filament in the $(x-y)$ plane [see Fig. 2(a)] and \vec{r}_b the

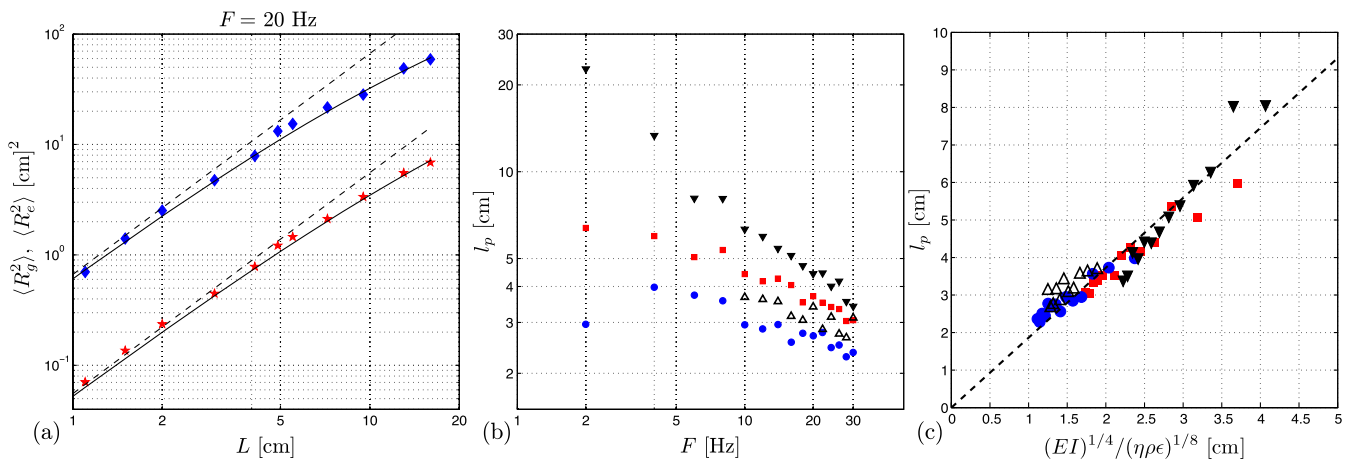


FIG. 2 (color online). (a) Evolution of $\langle R_e^2 \rangle$ (\blacklozenge) and $\langle R_g^2 \rangle$ (\star) as a function of the fiber length L (type I) at $F = 20$ Hz. Dashed and solid lines represent the prediction for rigid fibers and the fit from the wormlike chain model, respectively. (b) Evolution of the persistence length l_p as a function of the rotation frequency. (c) Evolution of the experimental persistence length l_p as a function of the characteristic length l_p^0 for $F \geq 4$ Hz. Dashed line is a guide to the eye with a slope of 1.9. F (\blacksquare) type I fiber, for (\bullet) type II fiber, (\blacktriangledown) type III fiber, (\triangle) type III fiber in Ucon + water mixture.

position of the projected barycenter as defined earlier and taking into account the 2/3 correction. In order to draw an analogy with polymers, the evolution of the end-to-end vector is compared to predictions of polymer models. After the classical random walk model of an ideal chain, which gives $\langle R_e^2 \rangle^{1/2} \propto N^{1/2}$, where N is the number of monomers in the chain, the most popular model is the self-avoiding random walk derived by Flory which predicts a scaling $\langle R_e^2 \rangle^{1/2} \propto N^{3/5}$ [12]. However, this model is not totally satisfactory here, as it requires a very long chain, which is not the case in our experiment as the fiber length stays close to the transition length. Kratky and Porod proposed a wormlike chain model for short semiflexible polymers [13], which seems much more appropriate to describe our system. In the limit of a continuous polymer, the end-to-end vector $\vec{R}_{e,3D}$ can be characterized by a persistence length l_p :

$$\langle R_{e,3D}^2 \rangle = 2l_p L - 2l_p^2 \left[1 - \exp\left(-\frac{L}{l_p}\right) \right]. \quad (3)$$

A similar formula can be calculated for $\langle R_g^2 \rangle$ [11] and gives here the same value of the persistence length. In polymer theory, l_p is the correlation length of the orientation along the polymer chain and is characteristic of the polymer flexibility: $l_p = \kappa/k_B T$, where κ is the bending modulus of the polymer and $k_B T$ the thermal energy. For short chains, $L \ll l_p$, $\langle R_{e,3D}^2 \rangle = L^2$, the polymer is similar to a rigid rod. Whereas for long chains, $L \gg l_p$, $\langle R_{e,3D}^2 \rangle = 2l_p L$, which corresponds to a pure random walk (ideal chain model). In our case, Eq. (3) has to be multiplied by 2/3 to take into account the projection. The persistence length is a free parameter used to fit experimental data which depends on the turbulence intensity $l_p(F)$. A very good agreement between the wormlike chain model and our experimental data is shown in Fig. 2(a). It proves that a flexible fiber in a turbulent flow wriggles as a wormlike-chain polymer in a good solvent.

To go further in the analogy, we will focus on the evolution of the persistence length when the turbulence intensity is increased. As we saw previously, in polymer theory, this length is defined by the balance of thermal energy and elastic energy. If it was the case here, turbulent fluctuations would play the role of thermal fluctuations and $k_B T$ should be replaced by the turbulent energy at scale ℓ $E_\ell \approx \frac{1}{2} \rho \ell^3 \epsilon^{2/3} \ell^{1/3}$. In both cases, the bending energy is $E_b(\ell) = \kappa/\ell$, where for a fiber, $\kappa = EI$ with I the area moment of inertia ($I = \pi d^4/64$ for a cylinder of diameter d [6]). So, the persistence length would be defined by $E_{l_p^E} = E_b(l_p^E)$ and so $l_p^E = (2EI/\rho)^{3/14} \epsilon^{-1/7}$. Unfortunately, the analogy is not so straightforward as l_p^E does not depend on the dynamic viscosity of the fluid η contrary to experimental measurements, cf. Fig. 2(b) for nylon fibers in water (▼) and in a water + Ucon mixture with viscosity $\eta = 100 \pm 12 \text{ mPa} \cdot \text{s}$ (Δ).

This dependence can be taken into account by considering the characteristic times of both the fiber relaxation and the turbulent forcing. Indeed, in polymer theory, as the thermal forcing is delta correlated, it exists only one time scale due to the polymer relaxation. On the contrary, the forcing due to turbulence is not delta correlated and we have to take into account another time corresponding to the lifetime of an eddy of size ℓ . This argument leads us to consider the power needed to bend a fiber in a flow instead of the required amount of energy. The relaxation time of the fiber can be estimated from the elastica equation:

$$\rho_f S \partial_{tt} \vec{y} + EI \partial_{ssss} \vec{y} = \vec{F}_D + \vec{F}_H, \quad (4)$$

where \vec{y} is the displacement from the equilibrium position, s the curvilinear coordinate along the fiber, ρ_f the fiber density, S its cross section, and \vec{F}_D and \vec{F}_H are, respectively, the drag force and all other hydrodynamics forces such as the added mass term, the Faxén force, and the history term. The relaxation time is only related to the dissipation of energy and thus to the drag force. Because the Reynolds number Re_d based on the slip velocity $\vec{u} - \partial_t \vec{y}$ and the diameter d of the fiber is relatively small, $Re_d = |\vec{u} - \partial_t \vec{y}| d / \nu \approx (d/\eta \kappa)^{4/3} \lesssim 300$, a first-order approximation is to assume that the drag force is proportional to the velocity as it is the case in the viscous regime. Therefore, Eq. (4) becomes

$$\rho_f S \partial_{tt} \vec{y} + \alpha \partial_t \vec{y} + EI \partial_{ssss} \vec{y} = \alpha \vec{u} + \vec{F}_H, \quad (5)$$

where $\alpha \propto \eta$ [14]. Equation (5) is a Langevin equation similar to the one used to describe polymer dynamics [15] but with a random forcing $\alpha \vec{u} + \vec{F}_H$ correlated in space and time. The relaxation time is given by $\tau = \alpha \ell^4 / EI \propto \eta \ell^4 / EI$, and so the power needed to bend the filament scales as $P_b(\ell) = (EI)^2 / \alpha \ell^5$. Note that we consider here an inextensible filament because the relaxation time scale of the strain is $(d/L)^2$ smaller than the relaxation time scale of bending [16]. Following polymer theory, the persistence length is then proportional to ℓ_m defined by the balance between the turbulent power $P_\ell \sim \rho \ell^3 \epsilon$ and the bending power P_b ; thus,

$$l_p^E \propto \ell_m = (EI)^{1/4} / (\rho \eta \epsilon)^{1/8}. \quad (6)$$

As can be seen in Fig. 2(c), this scaling law that takes into account the fluid viscosity is in good agreement with the experimental data presented in Fig. 2(b). Similarly to wormlike-chain polymers, the persistence length l_p^E characterizes here the transition between the rigid regime for short filaments and the flexible regime for long ones. The dashed line in Fig. 2(c) has a slope of 1.9. This factor is related to the orientation correlation along the fiber: if we consider the simplest deformation of a fiber of length ℓ with a single radius of curvature ℓ_m , the correlation function is $\sin x/x$, with $x = \ell/\ell_m$ having a correlation length $l_p \approx 1.9 \ell_m$.

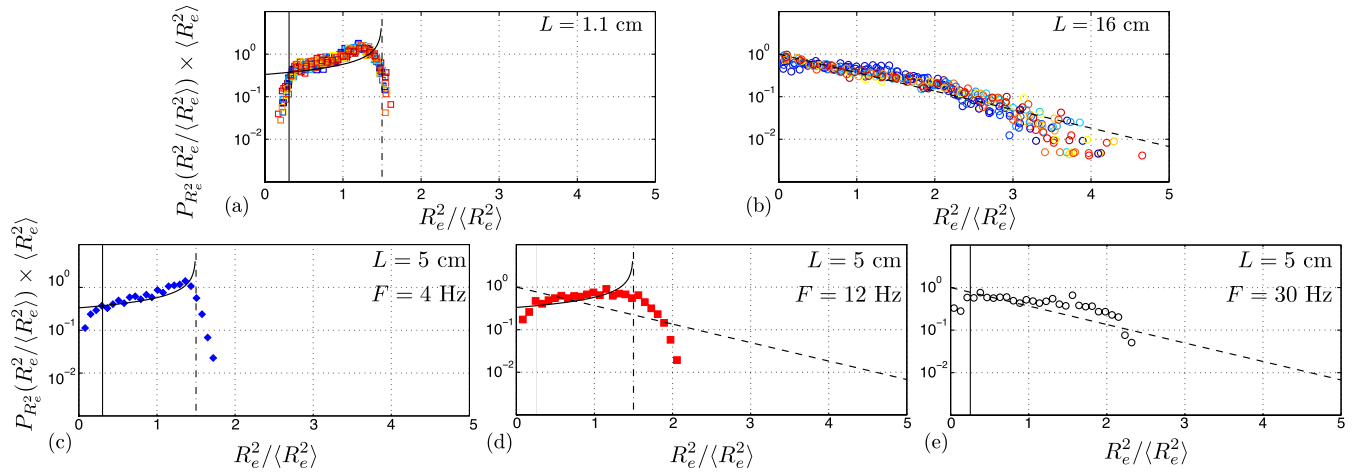


FIG. 3 (color online). PDF of $R_e^2 / \langle R_e^2 \rangle$ for fiber of type II. (a) Shortest length (rigid fiber), (b) long fiber (flexible filament), (c) intermediate length at small (c), intermediate (d), and high (e) rotation frequency and theoretical prediction of the PDF. Vertical lines are estimations of the minimal length detected by the image processing program (solid line) and the fiber length (dash-dotted line).

As can be seen in Fig. 1, the shape of the filament superimpositions is different for the rigid regime [1(c)] and the flexible one [1(d)]. To compare these fluctuations to the Gaussian distribution observed for the end-to-end vector of a flexible polymer [17], we study the evolution of the probability density function (PDF) of \vec{R}_e across the transition. As it was validated earlier, we still assume that the orientation and the norm of the end-to-end vector are independent. In that case, the PDF $P_{R_e^2}$ for a rigid fiber of length L is $P_{R_e^2} = 1/2L^2 \sqrt{1 - R_e^2/L^2} = 1/(2L^2 |\cos \theta|)$ [18], where θ is the angle between \vec{R}_e and the z axis ($R_e = L \sin \theta$, in the rigid case), whereas in the flexible regime, if the PDF was Gaussian, $P_{R_e^2} = \exp(-R_e^2 / \langle R_e^2 \rangle) / \langle R_e^2 \rangle$. In Fig. 3(a), the PDF for the shortest length of the type II fiber is shown. It is in good agreement with the predicted PDF of rigid rods for each rotation frequency F . This behavior is expected as the fiber length L is smaller than the persistence length l_p . On the other hand, Fig. 3(b) represents the PDF for one of the longest fibers, which is always in the flexible regime for any F . As can be seen in the figure, PDFs are close to the Gaussian distribution, as is the case in polymer theory. For an intermediate length, Figs. 3(c)–3(e) show that the PDF changes continuously from the rigid regime PDF to the Gaussian distribution depending on the value of $L/l_p(F)$. This Gaussian behavior in the flexible regime is consistent with the statistics of turbulence at large scales.

In conclusion, we have shown that the flexibility of a filament in a turbulent flow is negligible when its length is smaller than a typical length l_p . This persistence length, as it is called in polymer theory, depends on the fiber stiffness, the fiber relaxation time, and the injected power in the

turbulent flow. In the flexible regime, several similarities with a polymer in a good solvent have been enlightened. In particular, when the length of the fiber is increased, we proved that the evolution of the end-to-end vector or of the radius of gyration is identical to what is observed for wormlike-chain polymers. This similarity extends to the PDF of the end-to-end vector, at least when the length of the filament is close to the integral scale of the flow, as it was the case here. All presented results concern stationary statistics; the next step in considering a wriggled filament as a macroscopic polymer is to extend this analogy to its conformation dynamics. Additionally, this experiment might also permit us to tackle open questions in polymer science, such as the transition from the ideal chain model to the Flory regime [19], for instance.

This work has been carried out in the framework of the Labex MEC Project (No. ANR-10-LABX-0092) and of the A*MIDEX Project (No. ANR-11-IDEX-0001-02), funded by the “Investissements d’Avenir” French Government program managed by the French National Research Agency (ANR).

*Corresponding author.

gautier.verhille@irphe.univ-mrs.fr

- [1] A. Stohl, S. Eckhardt, C. Forster, P. James, N. Spichtinger, and P. Seibert, *Atmos. Environ.* **36**, 4635 (2002).
- [2] F. Lundell, D. L. Soderberg, and H. P. Alfredsson, *Annu. Rev. Fluid Mech.* **43**, 195 (2011).
- [3] S. Parsa, E. Calzavarini, F. Toschi, and G. A. Voth, *Phys. Rev. Lett.* **109**, 134501 (2012).
- [4] M. Shin and D. L. Koch, *J. Fluid Mech.* **540**, 143 (2005).
- [5] A. Pumir and M. Wilkinson, *New J. Phys.* **13**, 093030 (2011).
- [6] L. D. Landau and E. M. Lifshitz, *Theory of Elasticity* (Pergamon Press, New York, 1970).

- [7] A good solvent is by definition a solvent where the monomer-monomer, monomer-solvent, and solvent-solvent interactions are very close, cf. Ref. [10], p. 71.
- [8] F. Ravelet, Ph.D. thesis, CEA Saclay, 2005.
- [9] O. Cadot, S. Douady, and Y. Couder, *Phys. Fluids* **7**, 630 (1995).
- [10] P.-G. de Gennes, *Scaling Concepts in Polymer Physics* (Cornell University Press, Ithaca, NY, 1979).
- [11] H. Yamakawa, *Modern Theory of Polymer Solution* (Harper & Row, New York, 1971).
- [12] P.J. Flory, *Principles of Polymer Chemistry* (Cornell University Press, Ithaca, NY, 1953).
- [13] O. Kratky and G. Porod, *Recl. Trav. Chim.* **68**, 1106 (1949).
- [14] R. G. Cox, *J. Fluid Mech.* **44**, 791 (1970).
- [15] O. Hallatschek, E. Frey, and K. Kroy, *Phys. Rev. E* **75**, 031905 (2007).
- [16] T. R. Powers, *Rev. Mod. Phys.* **82**, 1607 (2010).
- [17] M. Doi and S.F. Edwards, *The Theory of Polymer Dynamics* (Oxford University Press, Oxford, 1988).
- [18] A. Papoulis, *Probability, Random Variables, and Stochastic Processes* (McGraw-Hill, New York, 1991), 3rd ed. See Eq. (5-5) with $f_\theta = \sin \theta/2$.
- [19] H.-P. Hsu, W. Paul, and K. Binder, *Europhys. Lett.* **92**, 28003 (2010).